



Fermi National Accelerator Laboratory

FERMILAB-Pub-97/104

Measurement of the Rate Capability of SSPMs Using Visible Light

M. Gubinelli, M. Sorel, O. Tonet, G. Parlavecchio, M. Atac, M. Mishina and J. Valls

*Fermi National Accelerator Laboratory
P.O. Box 500, Batavia, Illinois 60510*

April 1997

Disclaimer

This report was prepared as an account of work sponsored by an agency of the United States Government. Neither the United States Government nor any agency thereof, nor any of their employees, makes any warranty, expressed or implied, or assumes any legal liability or responsibility for the accuracy, completeness, or usefulness of any information, apparatus, product, or process disclosed, or represents that its use would not infringe privately owned rights. Reference herein to any specific commercial product, process, or service by trade name, trademark, manufacturer, or otherwise, does not necessarily constitute or imply its endorsement, recommendation, or favoring by the United States Government or any agency thereof. The views and opinions of authors expressed herein do not necessarily state or reflect those of the United States Government or any agency thereof.

Distribution

Approved for public release; further dissemination unlimited.

Measurement of the rate capability of SSPMs using visible light

M. Gubinelli, M. Sorel, O. Tonet, G. Parlavecchio
M. Atac, M. Mishina, J. Valls

April 15, 1997

Abstract

The rate capability of Solid State PhotoMultipliers (SSPMs) has been studied for various combinations of temperature and bias voltage. Using a 635 nm laser diode flasher the measurement was made up to the single photoelectron rate of 12 MHz. Only slight decrease, less than several per cent, of the quantum efficiency was observed at 12 MHz whereas 10% drop of the gain was observed.

I Introduction

The Solid State Photomultiplier (SSPM) [1, 2] is a miniature cell (≤ 1 mm diameter) photodiode with high quantum efficiency ($\geq 80\%$), broad spectral response in visible range (500-700 nm), excellent time response (rise time ≤ 1 ns), and high multiplication ($\geq 2 \cdot 10^4$) still with extremely low noise count rate. The pulse-by-pulse gain is extremely stable so that one can distinguish peaks corresponding to the number of photoelectrons clearly separated up to ~ 10 PE. It only needs 6–7 V to operate. The only somewhat cumbersome requirement is that it needs to be operated at near liquid helium temperature (6–7.5 K) in order to reduce the thermal electron noise to manageable level (< 5 kHz for > 1 photoelectron); this is because the band gap of the impurity semiconductor (Si:As) is on the order of 0.05 eV. SSPMs can be used for optical read out elements for particle detectors that emit light output, including possible scintillating fiber trackers. One of the properties to be measured is the rate capability, especially in the harsh conditions to be expected in the future high-luminosity colliders. The purpose of this work is to explore the rate capability of SSPMs using visible light.

II SSPM¹

SSPMs are materialized by multiple layers of epitaxially-grown single-crystal silicon. The upper part of Fig.1 shows a schematic cross section of the device [1, 2]. Fabrication begins on a heavily doped silicon substrate, which serves electrically as cathode. The front contact of the device, provided with an antireflective coating, is on the left and the substrate on the right. The structure has both As-doped and undoped epitaxial layers and in the doped layers the As

¹The content of this section is heavily borrowed from Refs.[1, 2]

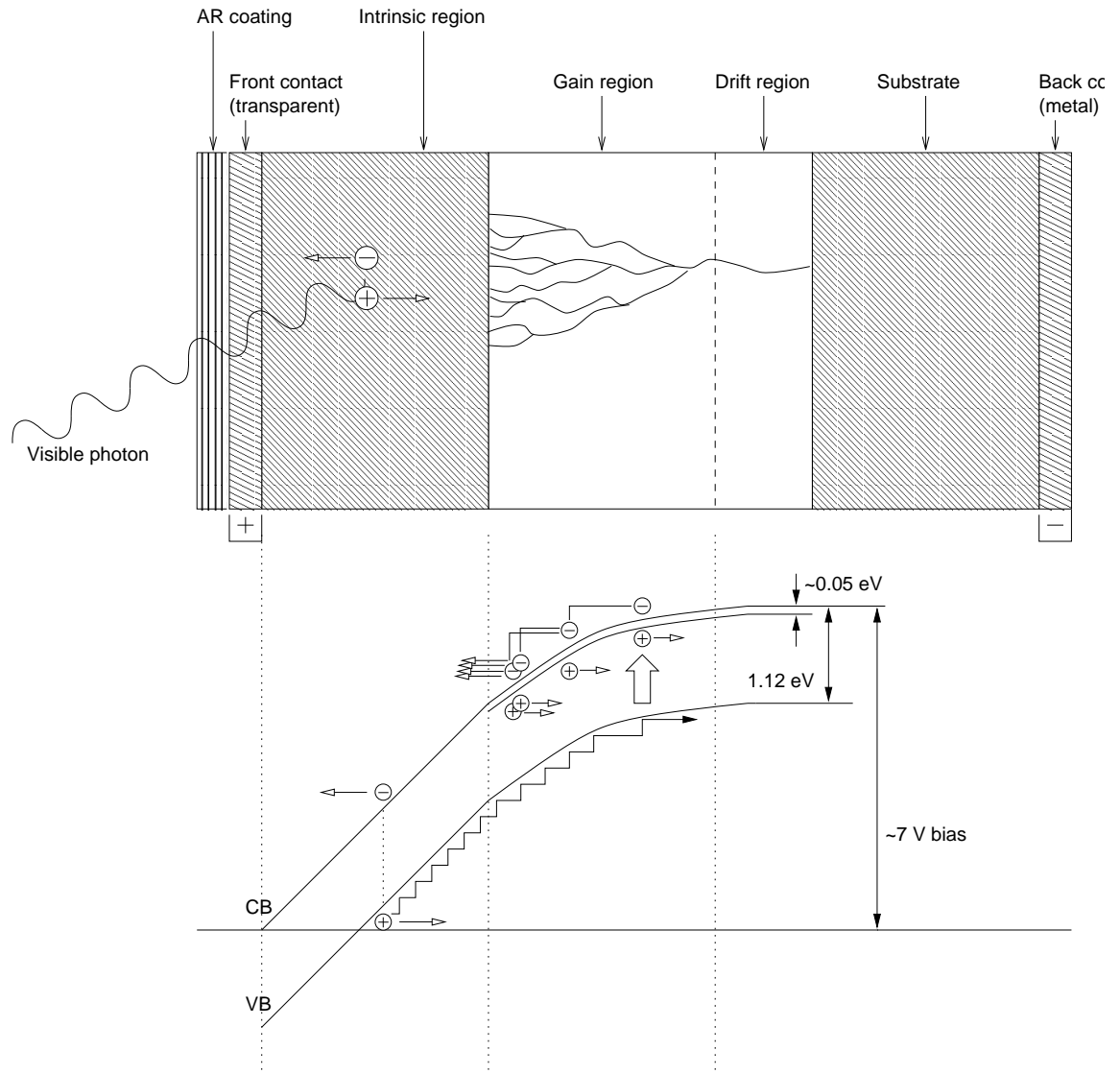


Figure 1: Structure of SSPM

dopant concentration is sufficiently high ($\geq 8 \cdot 10^{17} \text{cm}^{-3}$) for the formation of impurity bands: that means that donors or acceptors are so close together that, at low temperature, electrical transport may occur by charges hopping from impurity site to impurity site. It is this type of transportation, called Impurity Band Conduction, that makes this combination of features possible. Lower part of Fig.1 shows an electron-energy diagram for a typical device [1, 2]. The section on the left is not doped intentionally and contains only the conduction (CB) and the valence (VB) bands, with their 1.12 eV gap which, as usual in Si, dominates the optical absorption. The layers on the right also contain the impurity band, about 0.05 eV below the CB.

Visible photons enter from the left, are absorbed and create electron-hole pairs in the undoped region. The electrons move to the left and are collected at the front contact, whereas the holes move to the right, gaining kinetic energy up to the As doped region. There are some energy losses due to a series of scattering too small to cause impact ionization through the undoped region of 1.12 eV band gap. After reaching the gain region, however, each hole needs to acquire only 0.05 eV to impact-ionize an As atom and create an e^- - D^+ pair. The D^+ , analogous to a hole in intrinsic semiconductors, slowly moves to the right by hopping from an impurity atom to another and its probability of impact-ionize donors is negligible. Each e^- drifts to the left and soon ionizes another As atom, creating a second e^- - D^+ pair, and the avalanche grows rapidly as this process is repeated: by the time the avalanche reaches the edge of the As-doped region it contains several tens of thousands of electrons, which are swept rapidly to the left and collected at the front contact. A similar number of D^+ carriers are swept more slowly to the right and collected at the back contact. This small-gap avalanche has several desirable features: the electric field required is much lower than would be required for electron-hole multiplication through the 1.12 eV band gap and the resulting pulses have low gain dispersion. As a result, the output pulse height distribution has distinct peaks each corresponding to the initial number of photoelectrons. This is due to at least three factors: low scattering, single carrier multiplication and local field reduction. Scattering of holes in the doped region is low because impact-ionization across the 0.05 eV gap is so likely. The avalanche is of single-carrier type because D^+ move with a hopping process that gives up energy to the lattice by emitting phonons: thus D^+ carriers never acquire enough kinetic energy to ionize donors. Finally, localized field reduction limits the pulse height: when the avalanche grows, the attractive force between D^+ and e^- becomes significant compared to the static electric field and the avalanche gain is effectively limited.

III Cryogenic system for SSPM

SSPMs used for this measurement had $0.835\text{ mm} \times 0.835\text{ mm}$ square cells with a light-transmitting window on one side. The window has antireflective coating to minimize Fresnel loss of the incoming light. The window is conductive and serves as negative electrode, being connected to a plated pad on the side of each cell. A single row of eight such cells forms a chip with 0.9 mm spacing between the cells. The other side of the cells are aluminum plated as a common positive electrode.

In order to provide the required operating temperature, 6–7.5 K, SSPMs are housed at the bottom of a cassette which was inserted into the gas atmosphere above the liquid helium surface through the narrow neck at the top of an 8-liter cryostat. The structure of the cryostat is shown in Fig.2 and the structure of the cassette enlarged at the bottom portion is shown in Fig.3.

Each 8-cell SSPM chip is mounted on a gold-plated COVAR substrate with the commonly connected side epoxied with silver epoxy onto the substrate. Each pad on the other side is individually micro-wire bonded to a pin on the substrate. Four such substrates are then mounted on a shelving made of oxygen free high conductive (OFHC) copper at the bottom of the cassette.

Clear fibers are strung between a connector at the top of the cassette to four 8-fiber holders with the end of each fiber facing each of the SSPM cells. Naturally both ends of the fibers are cleanly cut by a diamond fly cutter. The gap between the SSPM surface and the end of the fiber

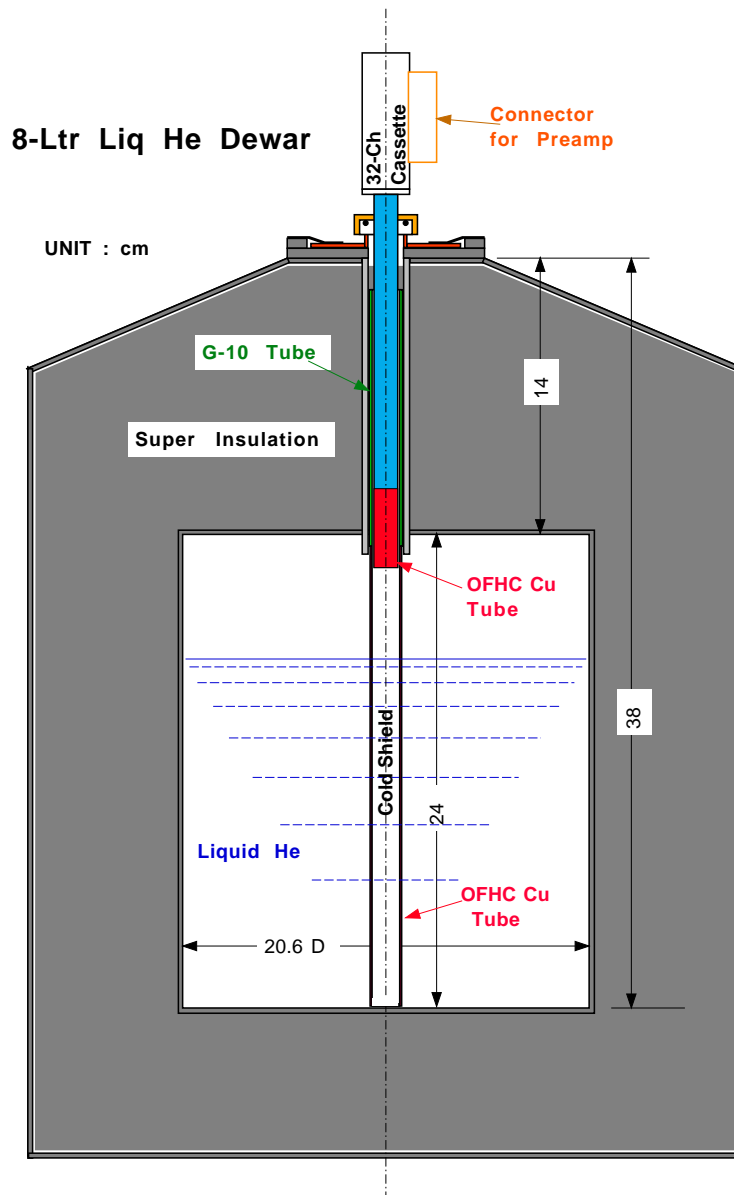


Figure 2: The structure of the 8-liter cryostat

is kept minimal, on the order of $50 \mu\text{m}$. It should be noted that the OFHC copper shelving is not fixed to the outer tube but suspended by the fibers, by means of COVAR fiber holders fixed on the shelving. With such a structure, when the cassette is cooled down the distance between the SSPMs and the end of the fibers does not change much.

It should also be pointed out that the clear fibers are natural blockers of infrared photons beyond $\sim 1.6 \mu\text{m}$ [3], as shown in Fig.4, for which the HMC devices, the version of SSPMs used in this measurement, still have some sensitivity though much reduced from original SSPMs.

The readout cables are connected to the pins on the substrates and brought up into the connector at the top of the cassette. The cables are made of stainless steel wires with teflon insulation and signal lines and ground lines are alternated in the ribbon. Because wires are

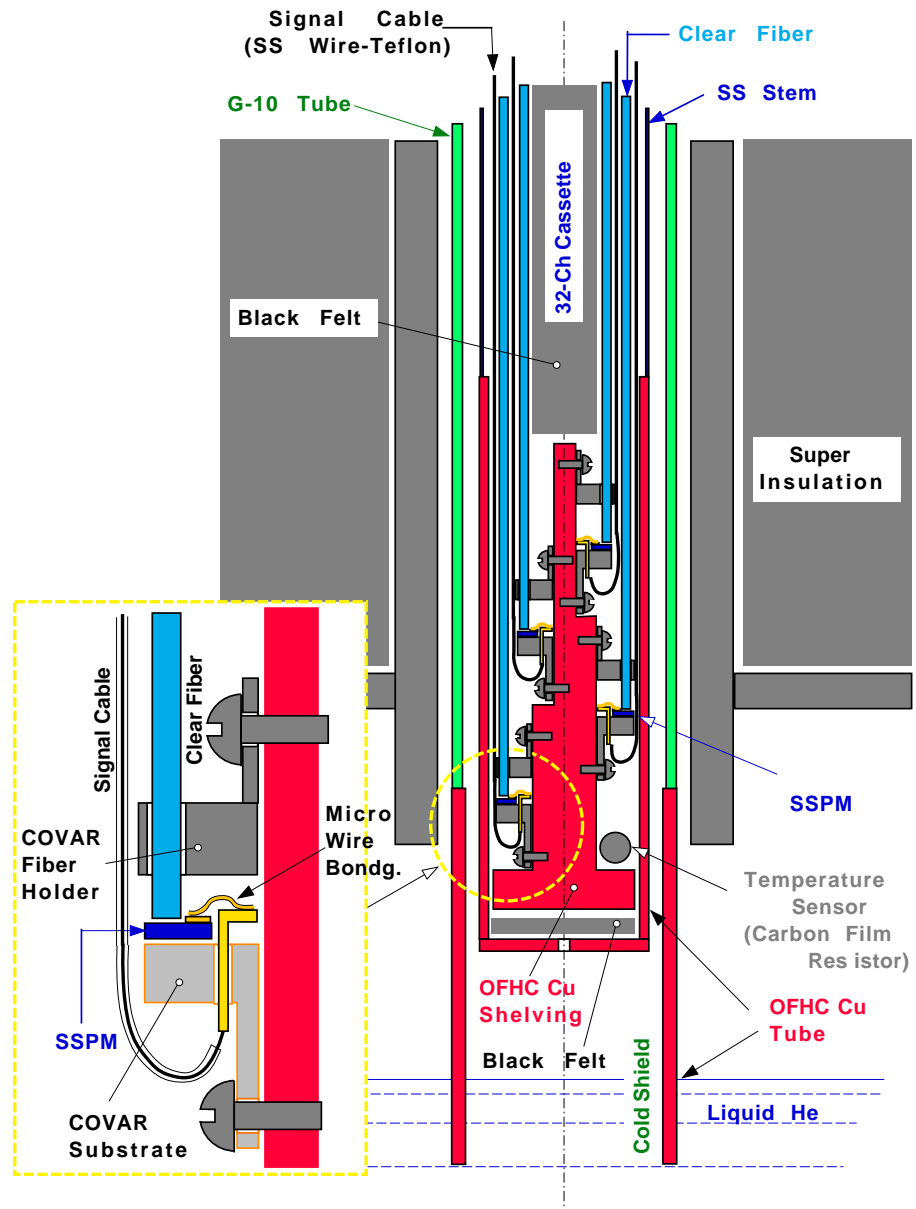


Figure 3: Enlarged view of the cassette

a significant contributor to the heat load of the cassette, stainless steel wires were chosen to minimize the heat leak. Ground lines are only grounded at the receiving end connected to a QPAO2 preamplifier card.

One of the lines is used to provide bias voltage common to all 32 channels being connected to the copper shelving. A 2 k Ω resistor was inserted at the end of the bias voltage line directly mounted on the copper shelving and a 0.1 μ F capacitor was connected between the copper shelving and the outer copper shield of the cassette as a filter. It was noticed that this arrangement

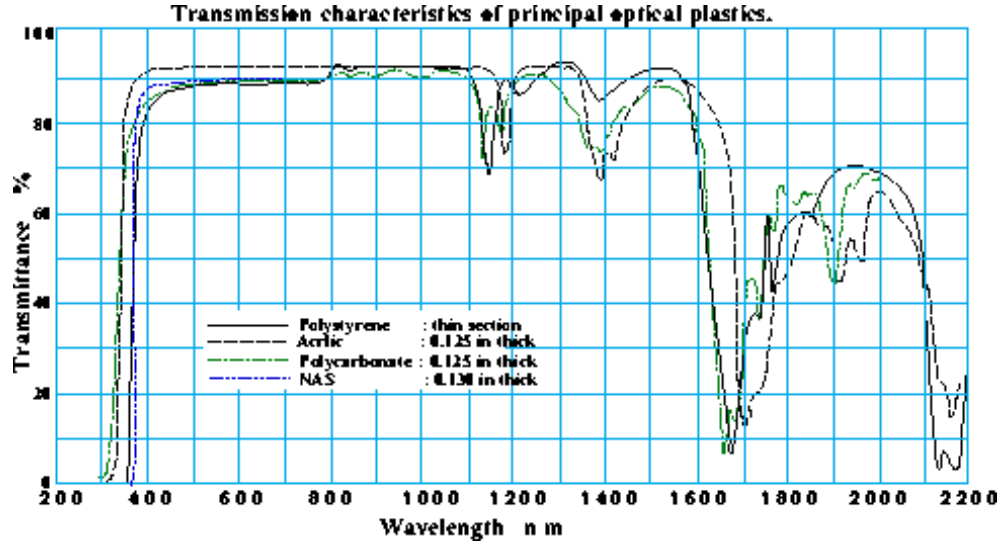


Figure 4: Transmission of polystyrene together with other optical plastics. (from Ref.[3])

greatly reduced the fluctuation of the signals, significantly improving the resolution of the pulse height spectrum of the signals.

The entire structure is then housed in a 13.85 mm cylinder made of a closed OFHC copper tube at the bottom 4 cm and the rest made of thin-wall stainless steel stem. The bottom lid of the copper tube has a small hole covered by a sheet of felt. The hole allows helium gas to rise through the inside of the cassette for precooling purpose to make full use of the enthalpy of the helium gas.

As shown in Fig.3 the cassette is inserted into the cold shield immersed in liquid helium in the cryostat. The bottom half of the cold shield is also made of OFHC copper tube to bring the liquid helium temperature (4.2 K) to the portion overlapping with the bottom copper tube of the cassette. A small gap between cassette and cold shield allows temperature gradient and minor adjustment of the height of the cassette can bring the SSPM temperature to required value. The temperature of the SSPM is measured by two carbon film resistors mounted on the copper shelving of the cassette. Due to such a structure, the total adjustment of the height of the cassette for full range of the liquid helium level is only ~ 4 cm, thus minimizing the signal cable length.

IV High rate measurement

IV.1 Rate testing method

In the hadron collider environment, the major source of the hits on each detector element is from minimum bias events, whose cross section is on the order of 50 mb.

Taking the IFT conceived for CDF as an example, the rate per element may be up to several hundreds of kHz in the severest case. The present measurement was designed to test SSPM up

to and beyond such range of the rate in mind.

The rate limitation may come from the following mechanism: each photon from the incident signal light pulse hits a spot in the SSPM cell and knocks out an electron with the probability corresponding to the quantum efficiency. Each electron starts an avalanche in high-field zone which creates electrical signal between the two electrodes on the surface. The avalanche stops when the field is saturated by the slowly-moving positively-charged donors. The local spot is insensitive until the donors are swept away into the negative electrode.

Preliminary simulations indicates that such local spot associated with a single avalanche is on the order of $15\ \mu\text{m}$ in diameter. The dead time of each of such spots indicated by original measurement was estimated to be around several tens of μsec . Because the local spot is small, the chance for a photon to hit exactly the spot paralyzed by a preceding hit is a matter of probability as a function of the average number of photons hitting a cell per unit time. Therefore the symptom to measure is the decrease of the quantum efficiency and of the avalanche gain as a function of the frequency of the input signals, as measured by the average number of photoelectrons per unit time. The above mentioned example of hit rate for the IFT then corresponds to several MHz as the single photoelectron (SPE) rate for average of about ten photons per track.

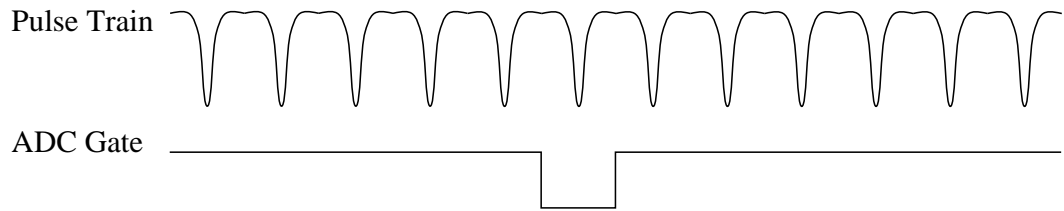


Figure 5: Rate measurement using single LED

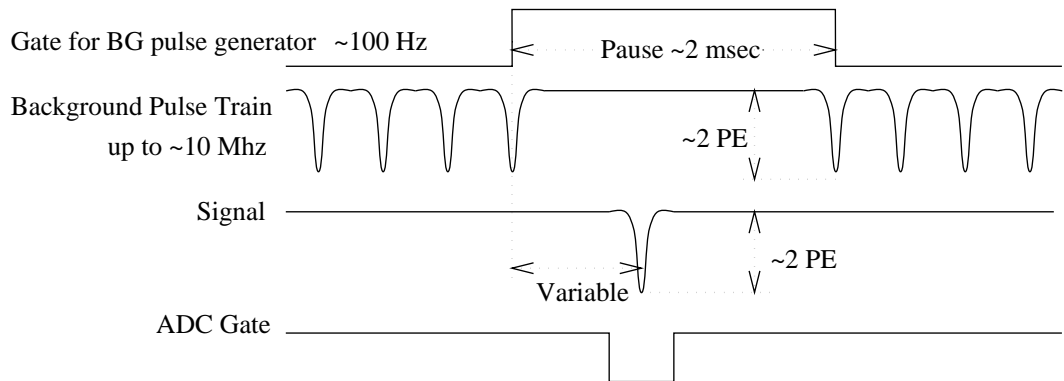


Figure 6: Rate measurement using two LEDs

Within the pause a signal pulse from another pulse generator was triggered at an adjustable timing up to 2 ms. The timing of the gate for the ADC² was adjustable so that the outputs from SSPMs are measured in time with signal pulse or with the first pulse of the background pulse train.

The timing and width of the gate pulse were tuned carefully to optimize the separation of the peaks in the pulse height spectrum which can be blurred by out-of-time photoelectron contribution that may be measured fractionally. The leading edge of the gate was set to a few nsec before the rising edge of the signal and the width was minimized down to ~ 30 ns.

IV.3 Choice of the light emitter

A major issue for the rate capability tests is to have light pulse sources with stable properties within the appropriate range of the frequencies and the input pulse heights. The width must be as short as possible in order to avoid adding significant contribution to the SSPM output pulse width, so that the gate width can be kept minimal.

A convenient way to fire SSPMs is to use LEDs of the wavelength matching to the spectral response of SSPMs. However we measured that most of the LEDs we tested had rather slow response. Eventually we found that Hitachi HL631MG laser diode had excellent properties. This device is a AlGaInP laser diode with a multi-quantum well structure and an emission spectrum that peaks at 635 nm, still within the broad peak of the SSPM response, though being in the red region.

IV.4 Testing laser diodes

To check the laser diode properties we used a Hamamatsu R2257 phototube [6]. The tube has a multialkali photocathode with its quantum efficiency plateau between 500 nm and 600 nm, as shown in Fig.8, and its response is fast, as shown in Fig.9 which shows the output pulse shape of the laser diode measured by the phototube. The results of the measurements for pulse height and full-width-at-half-maximum (FWHM) are plotted in Fig.10 and 11 showing a stable behaviour of the laser diode, both in light yield and in width of the pulse within the range of the frequency and the input pulse height, 1.8–2.3 V with 2.3 nsec width, used for the rate capabilities measurement.

IV.5 Measurement

A 32-channel preamplifier QPA02 was directly connected to the readout cable from the SSPMs at the top of the cassette. A typical example of the output signal from SSPMs, as amplified by QPA02, is shown in Fig.12 together with the ADC gate.

The preamplifier voltage was set at (4.0 ± 0.1) V and measurement was made for the following sets of the operating temperatures and bias voltages (V_{bias}):

²LeCroy 2249A CAMAC 10 bits ADC with 12 channels and a sensitivity of 0.25 pC/count.

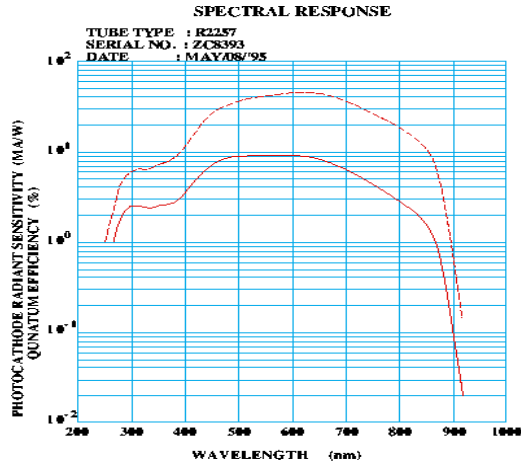


Figure 8: Quantum efficiency of R2257 (from Ref.[6])

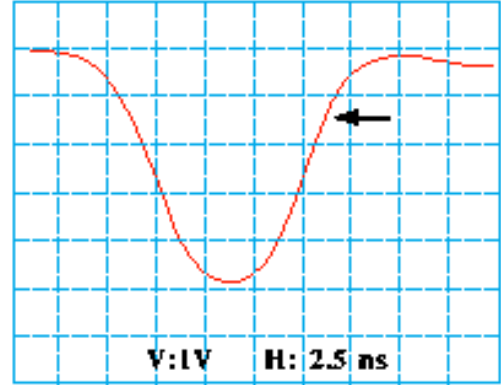


Figure 9: Laser diode output pulse shape, measured by R2257

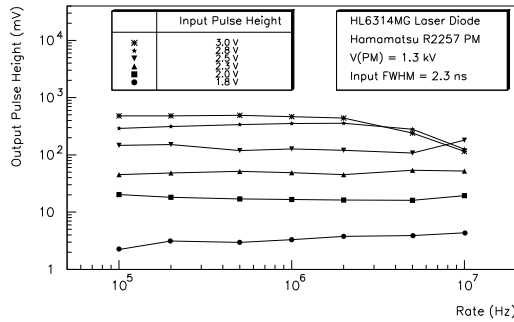


Figure 10: Laser diode output pulse height, measured by R2257

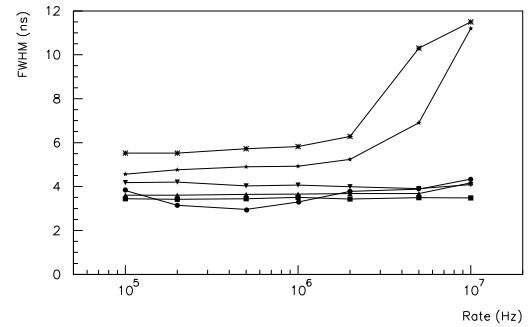


Figure 11: Laser diode output pulse FWHM, measured by R2257

| Temperature (K) | Bias voltage (V_{bias}) |
|-----------------------|-----------------------------|
| 7.5 (72 k Ω) | -6.0 |
| 6.9 (86 k Ω) | -6.5 |
| 6.5 (96 k Ω) | -6.5 -7.0 |
| 6.0 (112 k Ω) | -7.0 -7.5 |

For each condition of temperature and V_{bias} we took data of the SSPM response at 125 kHz, 625 kHz, 1.25 MHz, 2.5 MHz, and 6.25 MHz as the background frequency and for each of these frequencies we set the quiet time to 100 ns, 200 ns, 500 nsec, and 1 μ s. We also measured the signal without background pulse train for each of the different sets of temperature and V_{bias} for normalization and also the first pulse of the background pulse train after the pause in order to obtain the SPE rate of the background.

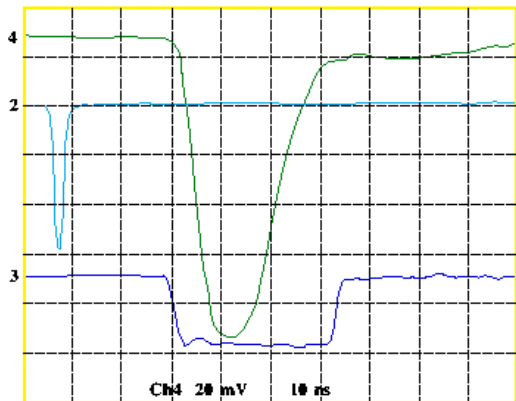


Figure 12: Output signal from SSPM

IV.6 Results

Each of the pulse height spectra of the SSPM output was fit by the following formula:

$$S(q) = \sum_{n=0}^{\infty} S_n(q) = N \sum_{n=0}^{\infty} G_n(q) \frac{(\overline{N_{pe}})^n}{n!} e^{-\overline{N_{pe}}}$$

$$G_n(q) = \frac{1}{\sqrt{2\pi}\sigma_n} \exp \left[-\frac{1}{2} \left(\frac{q - ped - n \cdot g}{\sigma_n} \right)^2 \right] ; \quad \sigma_n = \sqrt{\sigma_{ped}^2 + n \cdot \sigma_{gain}^2}$$

The free parameters in the fitting procedure are: the pedestal ped , its Gaussian spread σ_{ped} , the average gain of avalanches, g , its spread, σ_{gain} , and the average number of photoelectrons, $\overline{N_{pe}}$. The Gaussians convoluted with the Poissonian functions account for the fluctuation of the avalanche gain, read-out system dependent effects, and noise in the device. While fitting we used a partial summation up to $n = 15$. This model assumes a single averaged value g for all the gains g_n .

We tested whether this assumption was justified by a more flexible fitting function that leaves all the gains g_n as free parameters. Fig.13 and Fig.14 show the excellent matching of this kind of fit to the spectra and the linearity of their relative calibration curves for the overall gain ($g_n \sim \overline{g_i} \cdot n$) at operating conditions of the SSPM ($T=6.5$ K, $V_{bias}=-6.0$ V as a typical example). The figures are the data taken at SPE rate of 220 kHz and 11 MHz, respectively, with a quiet time of 100 ns. The larger error on the gain for the 7 PE peak (g_7) is due to the limited statistics of the samples with a total of 10,000 events. Up to 7 PE the overall gain is linear with respect to the number of photoelectrons, proving that no noticeable saturation occurs within the conditions we used for rate capability measurements. It should be noted that the preamplifier had a significantly limited dynamic range for the pulses corresponding to 8 PE or greater.

Using the fitting procedure described above we derived the following quantities for each set of conditions: $g, \sigma_g, \overline{N_{pe}}$, and ped . Those are plotted in Figs. 15 through 18. Figs. 19-A through

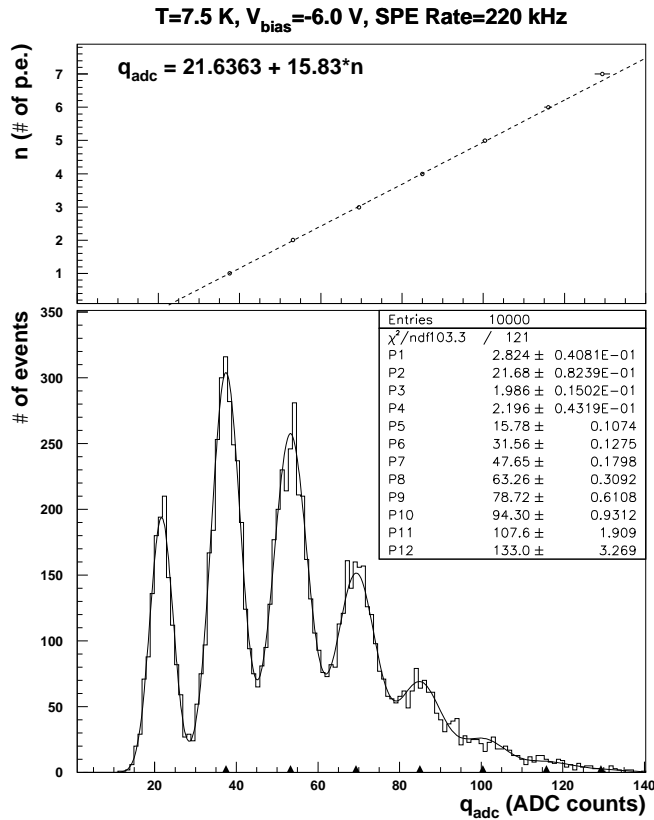


Figure 13: Test of gain linearity

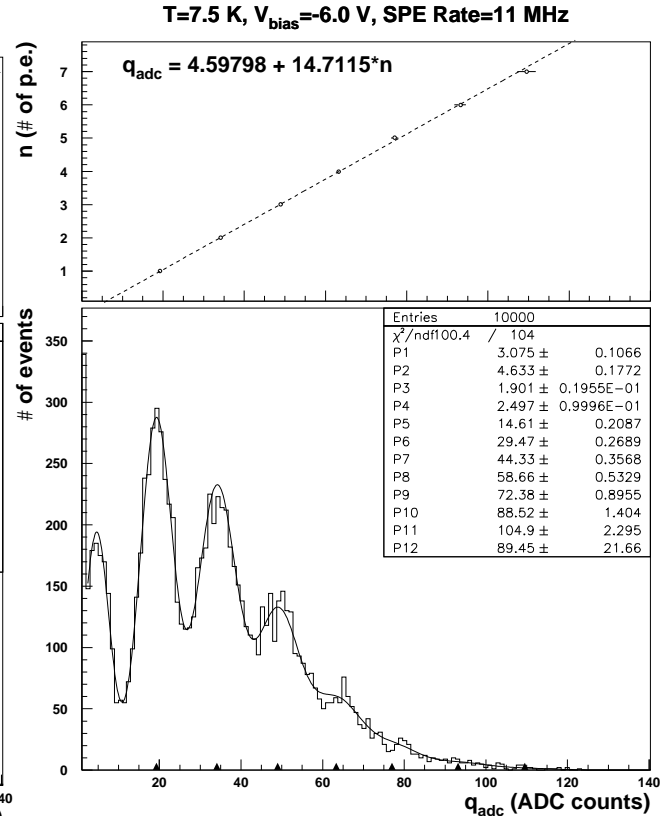


Figure 14: Test of gain linearity

19-D are the plots of the measured quantities as functions of the bias voltage at 240 kHz and 12 MHz.

As shown in Fig.19-A and Fig.19-B, higher bias voltage produces a major effect on the gain, which rises almost independently from the rate. However, since the absolute gain spread shows the same trend, this does not turn into a better peak resolution. On the other hand, a temperature increase gives, within the measured range of the operating conditions, a significantly improved and rate-independent relative gain spread.

Quantum efficiency increases with both the temperature and the bias voltage (Cf. Fig.19-C), and in both cases this behaviour is more significant at high rate.

Pedestal shift does not show a sizable dependence on the temperature nor the voltage (Cf. Fig.19-D) at low rate, while there is a striking increase of the shift going towards higher temperatures or bias voltages at higher frequencies.

Within the range of operating conditions we tested, gain shows a gradual decrease beyond 1MHz in SPE rate. The gain decrease at high frequency is obviously improved by increasing the temperature. In these ideal conditions, the gain reduction is only a few percent.

Quantum efficiency seems to be even less affected by rate: no visible effect can be noticed

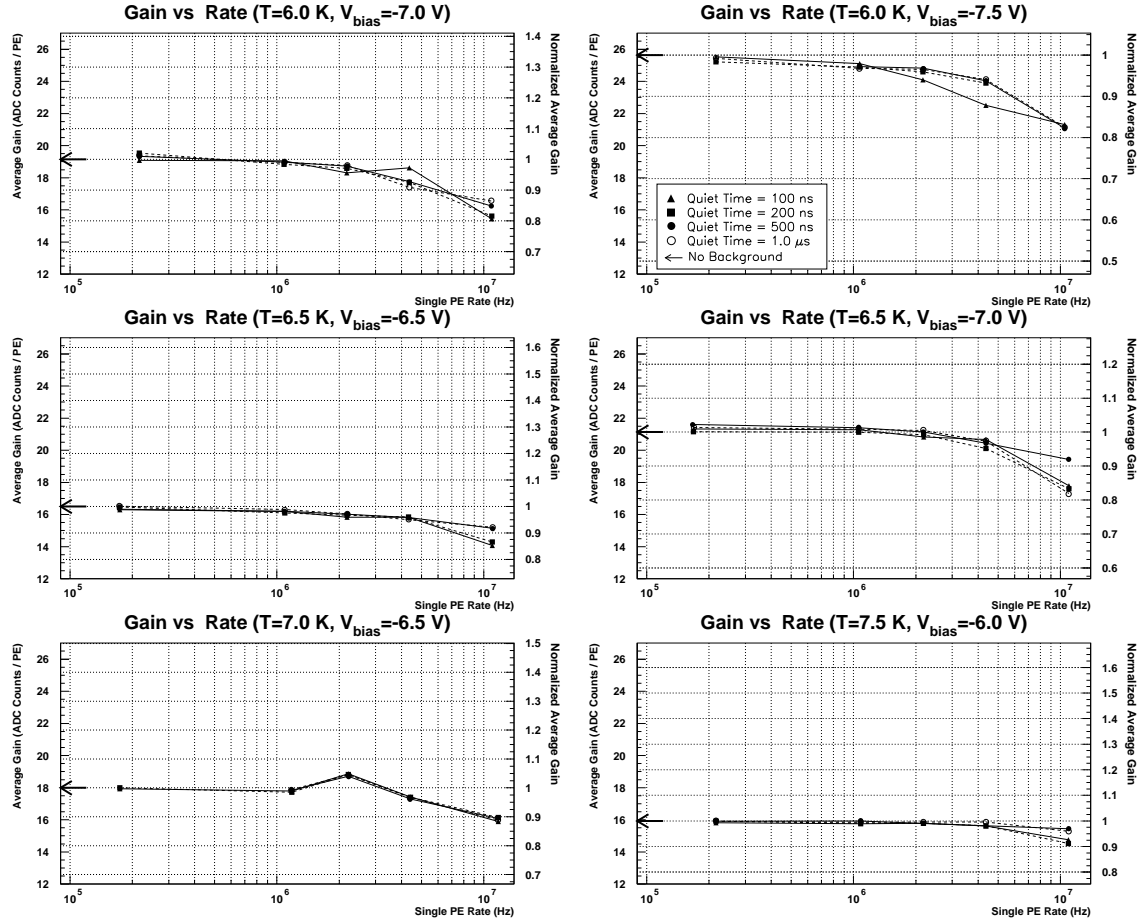


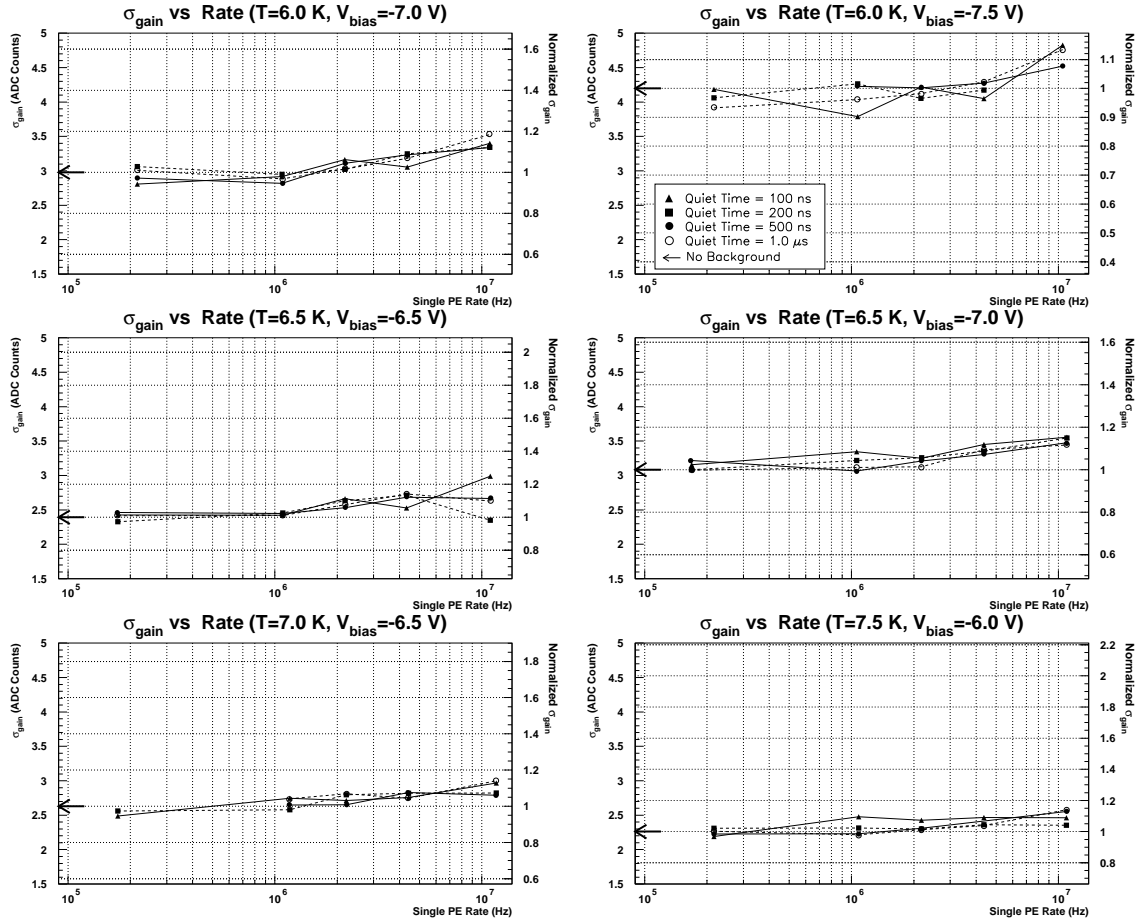
Figure 15: Gain vs Rate

up to 4 MHz SPE rate, and an overall trend of decrease for higher rates, which does not exceed several percent level at 12 MHz.

Keeping in mind the stability of the other fitting parameters, the pulse height spectra are somewhat globally shifted, due to pedestal shift, without significant change in their shape, when rate increases. It should be noted that such shift can be easily corrected by downloading adequate parameters dependent on the luminosity in the actual experiment.

V Conclusions

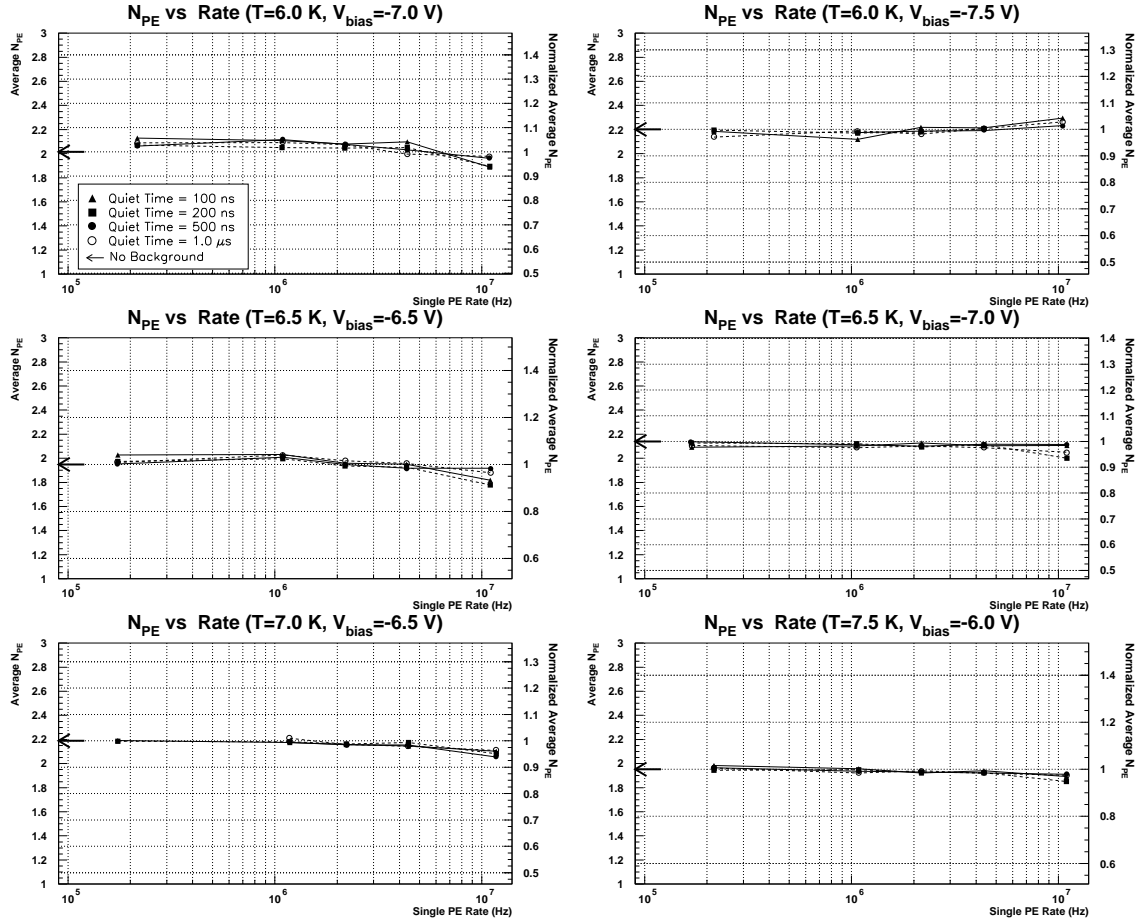
We have made a systematic study of the rate capability of SSPMs. The pedestal shift, gain, spread of the gain, and the number of photoelectrons were measured at temperature range between 6.0 K and 7.5 K with varying frequencies of the background pulse train up to 12 MHz. While a significant shift of the pedestal, which may be mostly due to outside circuitry, was

Figure 16: σ_{gain} vs Rate

observed, the gain and the spread of the gain exhibited a milder change with frequencies. The number of phototelctrons with fixed light input, which is interpreted as a quantum efficiency in relative scale, essentially does not change with the frequencies up to several MHz which is expected to be an upper limit of the rate of the proposed IFT in CDF's environment in Run II. Even at the highest frequency, 12 MHz, the measured change was only several percent for most sets of the temperature and bias voltage combinations.

VI Acknowledgements

M.G., M.S., O.T., and G.P. are grateful to Exchange Visitor Program #P3-5586 funded by INFN, Italy. The program gave them the opportunity to work on their project at Fermilab. We thank Drs. G. Piacentino and A. Parri for lectures provided to us. Prof. G. Bellettini gave us continuous encouragement throughout our stay at Fermilab. Special thanks go to Dr. F. Bedeschi

Figure 17: N_{PE} vs Rate

for organizing this program.

References

- [1] M. G. Staplebroek and M. D. Petroff, "Visible light photon counters for scintillating fiber applications: II. Principles of operation", *Proceedings of Scifi 93. Workshop on scintillating fiber detectors* (World Scientific, Singapore, 1993) 621.
- [2] G. B. Turner, et al., "Visible light photon counters for scintillating fiber applications: I. Characteristics and performance", *Proceedings of Scifi 93. Workshop on scintillating fiber detectors* (World Scientific, Singapore, 1993) 613.
- [3] U.S. Precision Lens, Inc., "The Handbook of Plastic Optics", Second Edition (3997 McMann Rd., Cincinnati, Ohio 45245).

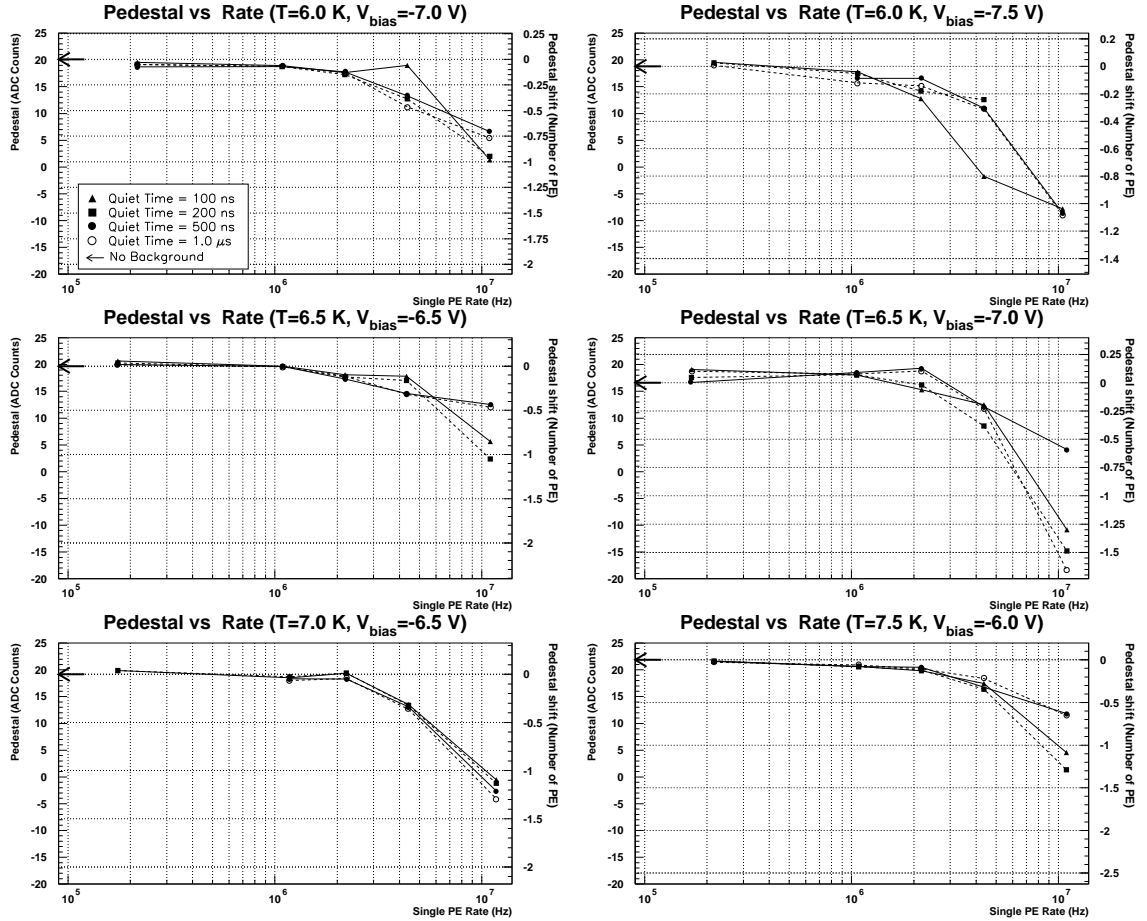


Figure 18: Pedestal vs Rate

- [4] Y. Kato, Private communication.
- [5] J. A. Valls, M. Atac, and M. Mishina, “Study of the performance of SSPMs at high rates”, *CDF note 3790*.
- [6] Hamamatsu Photonics data sheet.

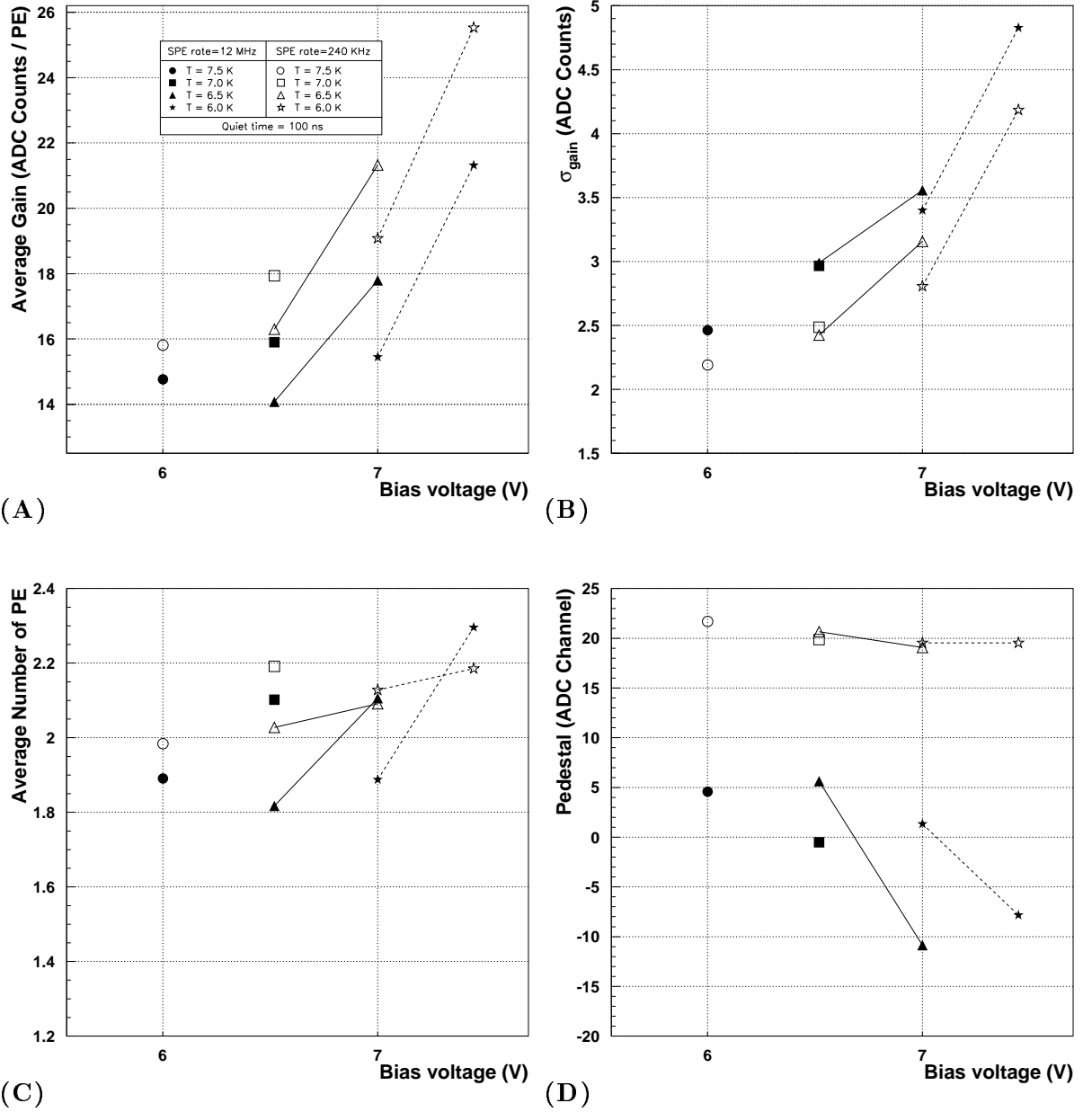


Figure 19: Measured quantities as function of V_{bias}